Supplementary Material: Vertex function compliant with the Ward identity for quasiparticle self-consistent calculations beyond *GW*

Alexey Tal,[1,*] Wei Chen,[2] and Alfredo Pasquarello[1]

[1] *Chaire de Simulation à l'Echelle Atomique (CSEA), Ecole Polytechnique Fédérale de Lausanne (EPFL), CH-1015 Lausanne, Switzerland*

[2] *Institute of Condensed Matter and Nanoscience (IMCN), Université catholique de Louvain, B-1348 Louvain-la-Neuve, Belgium*

[*] alexey.tal@epfl.ch

I. COMPUTATIONAL DETAILS

The calculations are performed with the projector augmented wave (PAW) method [1] implemented in VASP [2, 3]. QSGW calculations with the nanoquanta vertex corrections are performed starting with G_0W_0 energies, wave functions, and dielectric matrices. All other QSGW calculations are performed starting from PBE. To achieve convergence, six iterations are performed. The derivative of the cell-periodic part of the orbitals w.r.t. the **k**-points is calculated with the PEAD method [4].

The Al_sv_GW, O_GW_new, As_d, N_GW_new, P_GW, Ar_GW, B_GW, C_GW_new, Ca_sv_GW, Cd_sv_GW, S_GW, Se_sv_GW, Ga_d_GW, Ge_d_GW, In_d_GW, Li_sv_GW, Cl_GW, F_GW_new, Mg_sv_GW, Si_sv_GW, and Zn_sv_GW ultrasoft PAW (US-PAW) potentials are used in the calculations. The semicore states are included in the case of (post-)transition metals.

Comparison of the band gaps calculated with the norm-conserving potentials in the $G\widetilde{W}^{\mathrm{NQ}}$ approximation provided in Ref. [5] shows that the choice of potentials has no major effect on the band gaps with a mean error of 0.08 eV. On the other hand, the use of the US-PAW pseudopotentials can lead to a substantial error for the energy levels of the d bands [6]. Thus, in order to correct the d-band positions calculated with US-PAW, we apply the shift

$$\Delta = \varepsilon_d^{GW^{\mathrm{NQ}}}\left[\mathrm{US}-\mathrm{PAW}\right] - \varepsilon_d^{GW^{\mathrm{NQ}}}\left[\mathrm{NC}-\mathrm{PAW}\right],$$

where the values for $\varepsilon_d^{GW^{\mathrm{NQ}}}\left[\mathrm{NC}-\mathrm{PAW}\right]$ are taken from Ref. [5]. The corrections Δ are given in Table V.

Thomas-Fermi vectors are calculated as a macroscopic average of the electron density over the unit cell. In the transition metals, d electrons are included in the valence which can lead to an overestimation of k_{TF} in such systems.

II. CONVERGENCE

The convergence parameters of the calculations are provided in Table I. The ionization potentials are calculated by correcting the PBE values taken from Ref. [5] with QP shifts. These corrections are calculated for the infinite basis set through the extrapolation scheme described in Ref. [6]. The calculations of the dielectric constant require denser **k**-point

meshes than the QP energies. The grid used in the present work ensures convergence within 0.1 for LiF, LiCl, MgO, CaO, ZnO, BN, ZnS, GaN, CdS, CdSe, C, ZnSe, SiC, AlP, and AlAs. In the case of GaP, InP, GaAs, and Si, the dielectric constants are converged within 0.5.

By focusing on BN and MgO, we show in Fig. 1 that the presence of the $f_{\rm xc}^{\rm LR+LDA}$ vertex in the self-energy and the polarizability does not cause any instabilities in the convergence.

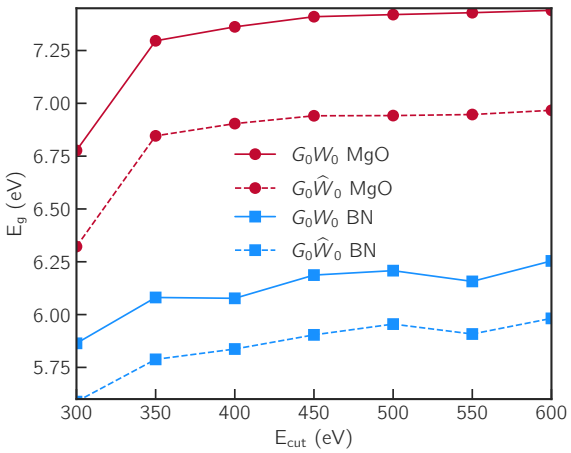

FIG. 1. Convergence of the band gaps with and without vertex corrections.

III. VERTEX CORRECTIONS

In reciprocal space the response function χ_0 is defined as follows

$$\chi_{0\mathbf{G},\mathbf{G}'}(\mathbf{q},\omega) = \frac{1}{\Omega}\sum_{nn'\mathbf{k}} 2w_{\mathbf{k}}\left(f_{n'\mathbf{k}+\mathbf{q}} - f_{n'\mathbf{k}}\right) \times \frac{\left\langle \psi_{n'\mathbf{k}+\mathbf{q}} \left| e^{i(\mathbf{q}+\mathbf{G})\mathbf{r}} \right| \psi_{n\mathbf{k}} \right\rangle \left\langle \psi_{n\mathbf{k}} \left| e^{-i(\mathbf{q}+\mathbf{G}')\mathbf{r}'} \right| \psi_{n'\mathbf{k}+\mathbf{q}} \right\rangle}{\epsilon_{n'\mathbf{k}+\mathbf{q}} - \epsilon_{n\mathbf{k}} - \omega - i\eta}. \tag{1}$$

Here Ω is the volume of the system, $w_{\mathbf{k}}$ is the weight of the k point, and the $f_{n\mathbf{k}}$ are the one electron occupancies of the states $(n, \mathbf{k})$, η is a positive infinitesimal, the factor of 2 is due to the spin-degenerate systems considered here, and the band indices n and n' run over all the bands.

The behavior of Γ in $q \to 0$, $\omega \to 0$ limit is given by the first Ward identity, which connects the vertex and the renormalization factor $\Gamma = 1/Z$. Hence, we find a static xc kernel in the long-range limit

$$\lim_{\mathbf{q}+\mathbf{G}+\mathbf{G}'\to 0} \Gamma = \frac{1}{1 - f_{\rm xc}^{00}(\mathbf{q}\to 0, \omega\to 0)\chi_0^{00}(\mathbf{q}\to 0, \omega\to 0)} = \frac{1}{Z(\mathbf{q}\to 0, \omega\to 0)}, \tag{2}$$

where the indices 00 indicate the head of the matrix. Considering that $f_{\rm xc}^{00}$ and χ_0^{00} are scalar functions, we find the static long-range xc kernel

$$f_{\rm xc}^{\rm LR}(\mathbf{q}\to 0,\omega\to 0) = \frac{1-Z(\mathbf{q}\to 0,\omega\to 0)}{\chi_0^{00}(\mathbf{q}\to 0,\omega\to 0)} \tag{3}$$

The ALDA kernel in reciprocal space is obtained via the Fourier transform

$$f_{{\rm xc},\mathbf{G},\mathbf{G}'}^{\rm LDA} = \frac{1}{\Omega}\int_\Omega {\rm d}\mathbf{r} e^{-i(\mathbf{G}-\mathbf{G}')\cdot\mathbf{r}} f_{\rm xc}\left[n(\mathbf{r})\right], \tag{4}$$

where, Ω is the volume of the unit cell.

The vertex of the QS$G\widehat{W}$ scheme reads

$$f_{{\rm xc},\mathbf{G},\mathbf{G}'}^{\rm LR+LDA}(\mathbf{q},\omega) = \frac{1-Z(\mathbf{q}=0,\omega=0)}{\chi_0^{00}(\mathbf{q},\omega=0)} e^{-|\mathbf{q}+\mathbf{G}|^2/k_{\rm TF}^2}\delta_{\mathbf{G},\mathbf{G}'} + f_{{\rm xc},\mathbf{G},\mathbf{G}'}^{\rm LDA}(1-e^{-|\mathbf{q}+\mathbf{G}|^2/k_{\rm TF}^2})\delta_{\mathbf{G},\mathbf{G}'} \tag{5}$$

TABLE I. Convergence parameters and structures used in the calculations. The structures are the same as in Ref. [7]. Z is the converged renormalization factor corresponding to the VBM.

	$E_{\text{cutoff}}^{\text{DFT}}$(eV)	$E_{\text{cutoff}}^{\text{GW}}$(eV)	N_ω	N_{bands}	k-points	Space group	a_0(Å)	c_0/a_0	Z
AlAs	500	333	150	512	$6\times6\times6$	$F\bar{4}3m$	5.661		0.79
AlP	500	333	110	512	$6\times6\times6$	$F\bar{4}3m$	5.451		0.79
Ar	600	400	90	1024	$6\times6\times6$	$Fm\bar{3}m$	5.26		0.89
BN	500	333	110	512	$6\times6\times6$	$F\bar{4}3m$	3.616		0.84
C	500	333	50	512	$6\times6\times6$	$Fd\bar{3}m$	3.567		0.84
CaO	400	266	110	256	$6\times6\times6$	$Fm\bar{3}m$	4.803		0.81
CdS	500	333	150	512	$6\times6\times6$	$F\bar{4}3m$	5.818		0.79
CdSe	500	333	150	512	$6\times6\times6$	$F\bar{4}3m$	6.052		0.79
Cu_2O	500	333	150	512	$4\times4\times4$	$Pn\bar{3}n$	4.269		0.68
GaAs	500	333	130	1024	$6\times6\times6$	$F\bar{4}3m$	5.648		0.80
GaN	500	333	70	1024	$6\times6\times6$	$P6_3mc$	3.189	1.626	0.80
GaP	500	333	90	1024	$6\times6\times6$	$F\bar{4}3m$	5.448		0.78
InP	500	333	150	512	$6\times6\times6$	$F\bar{4}3m$	5.866		0.77
LiCl	500	333	70	512	$6\times6\times6$	$Fm\bar{3}m$	5.106		0.85
LiF	600	400	50	1024	$6\times6\times6$	$Fm\bar{3}m$	4.010		0.87
MgO	500	333	130	512	$6\times6\times6$	$Fm\bar{3}m$	4.207		0.83
Si	600	400	128	512	$6\times6\times6$	$Fd\bar{3}m$	5.430		0.77
SiC	600	400	110	512	$6\times6\times6$	$F\bar{4}3m$	4.358		0.82
ZnO	500	333	200	1024	$4\times4\times4$	$P6_3mc$	3.250	1.601	0.92
ZnS	500	333	150	512	$6\times6\times6$	$F\bar{4}3m$	5.410		0.80
ZnSe	500	333	150	512	$6\times6\times6$	$F\bar{4}3m$	5.667		0.81

TABLE II. Calculated band gaps (in eV). Experimental band gaps and zero-phonon renormalizaton (ZPR) corrections are taken from Ref. [7].

	QSGW	QS$G\widetilde{W}^{\mathrm{Boot}}$	QS$G\widetilde{W}^{\mathrm{NQ}}$	QS$G\widetilde{W}^{\mathrm{LR}}$	QS$G\widehat{W}$	Expt.+ZPR
AlAs	2.66	2.47	2.40	2.48	2.39	2.28
AlP	2.90	2.67	2.54	2.66	2.56	2.54
Ar	14.90	13.89	14.38	14.87	14.23	14.33
BN	6.99	6.49	6.44	6.68	6.59	6.74
C	6.18	5.82	5.86	5.89	5.83	5.85
CaO	7.43	6.68	6.82	7.04	6.79	7.09
CdS	2.97	2.52	2.62	2.58	2.38	2.64
CdSe	2.30	1.95	1.96	2.03	1.84	1.88
Cu_2O[a]	2.79	2.37	1.99	2.33	1.79	2.17
GaAs	1.83	1.62	1.64	1.70	1.58	1.57
GaN	4.18	3.73	3.65	3.81	3.61	3.67
GaP	2.70	2.49	2.39	2.48	2.41	2.43
InP	1.75	1.53	1.54	1.54	1.42	1.47
LiCl	10.46	9.66	9.61	10.15	9.87	9.57
LiF	16.28	14.58	15.26	15.95	15.52	15.35
MgO	9.03	8.03	8.19	8.57	8.37	8.36
Si	1.50	1.35	1.32	1.33	1.27	1.23
SiC	2.82	2.55	2.48	2.58	2.56	2.52
ZnO	4.15	3.42	3.69	3.77	3.41	3.60
ZnS	4.21	3.65	3.75	3.81	3.63	3.94
ZnSe	3.29	2.88	2.90	2.99	2.75	2.87
MAE	0.43	0.19	0.09	0.18	0.12	

[a] not included in the MAEs to allow for a consistent comparison with the results of Ref. [5], where this material had not been considered.

TABLE III. Ionization potentials (in eV). The ionization potentials are obtained as a QP correction to the PBE values taken from Ref. [5]. MAEs are calculated relative to the average experimental value when several references are available. Experimental values are taken from Refs. [8–11].

	PBE[a]	HSE[a]	$GW\Gamma$[a]	QSGW	QS$G\widetilde{W}^{\mathrm{Boot}}$	QS$G\widetilde{W}^{\mathrm{LR}}$	QS$G\widehat{W}$	Expt.
AlAs	5.32	5.83	6.37	6.52	6.51	6.44	5.69	
AlP	5.70	6.22	6.64	6.93	6.91	6.78	6.02	
BN	7.03	7.85	8.52	8.78	8.66	8.68	7.89	
C	5.58	6.18	6.74	6.96	6.91	6.87	6.12	5.85 6.00 6.5
CdS	5.92	6.60	7.17	7.51	7.33	7.30	6.60	6.10 7.26
CdSe	5.61	6.23	6.93	7.10	7.04	6.97	6.29	6.62
Cu_2O[b]	4.27	5.18		5.60	5.87	6.97	5.13	5.25
GaAs	4.84	5.32	5.77	5.88	5.89	5.85	5.06	5.40 5.47 5.56
GaN	5.92	6.61	7.12	7.64	7.52	7.39	6.64	6.60 6.80
GaP	5.26	5.75	6.13	6.37	6.37	6.30	5.50	5.95 6.01
InP	5.13	5.59	5.95	6.22	6.19	6.11	5.41	5.69 5.85
MgO	5.20	6.15	7.34	7.98	7.62	7.77	6.95	7.15
Si	4.82	5.22	5.49	5.72	5.73	5.66	4.93	5.15 5.33
SiC	6.03	6.64	7.00	7.29	7.26	7.18	6.41	5.90 6.00
ZnO	6.01	7.11	8.19	8.58	8.32	8.40	7.63	7.82
ZnS	6.03	6.77	7.43	7.75	7.56	7.54	6.79	7.50
ZnSe	5.62	6.29	7.06	7.23	7.15	7.08	6.37	6.82
MAE	0.92	0.37	0.36	0.65	0.54	0.51	0.31	

[a] from Ref. [5]

[b] not included in the MAEs to allow for a consistent comparison with the results of Ref. [5], where this material had not been considered. The PBE and HSE values are taken from Ref. [11].

TABLE IV. Calculated dielectric constants. Experimental values are taken from Ref. [7].

	QSGW	QS$G\widetilde{W}^{\mathrm{Boot}}$	QS$G\widetilde{W}^{\mathrm{NQ}}$	QS$G\widetilde{W}^{\mathrm{LR}}$	QS$G\widehat{W}$	Expt.
AlAs	6.06	7.01	7.72	7.52	8.21	8.16
AlP	5.51	6.42	7.02	6.85	7.47	7.54
Ar	1.47	1.70	1.59	1.49	1.57	1.66
BN	3.62	4.35	4.45	4.16	4.39	4.50
C	4.56	5.31	5.44	5.31	5.60	5.70
CaO	2.64	3.33	3.16	3.04	3.24	3.30
CdS	3.96	4.93	5.05	4.95	5.34	5.20
CdSe	4.55	5.54	5.69	5.61	6.20	5.80
GaAs	8.09	9.26	9.79	9.92	10.76	10.58
GaN	3.95	4.82	5.34	4.83	5.14	5.30
GaP	6.77	7.85	9.12	8.60	9.26	9.10
InP	6.95	8.13	8.74	9.08	9.86	9.60
LiCl	2.20	2.68	2.71	2.41	2.56	2.70
LiF	1.65	2.09	1.88	1.74	1.81	1.90
MgO	2.38	3.02	2.92	2.68	2.81	3.00
Si	8.96	10.12	11.23	11.56	12.35	12.00
SiC	5.22	6.12	6.46	6.33	6.59	6.52
ZnO	2.87	3.70	3.36	3.41	4.06	3.74
ZnS	3.98	4.94	5.00	4.87	5.23	5.13
ZnSe	4.53	5.48	5.62	5.50	5.97	5.90
MAE	1.37	0.55	0.26	0.37	0.16	

TABLE V. Mean position (in eV) of the semicore d states at the Γ point with respect to the VBM. The experimental values and the values calculated with the NC-PAW potentials are taken from Ref. [5].

	NC-PAW		US-PAW					
	$GW\Gamma$	$G\widetilde{W}^{\mathrm{NQ}}$	QS$G\widetilde{W}^{\mathrm{NQ}}$	QSGW	QS$G\widetilde{W}^{\mathrm{LR}}$	QS$G\widehat{W}$	Δ	Expt.
ZnO	7.10	6.90	6.60	7.28	6.72	6.81	0.30	7.50
ZnS	8.40	8.00	7.82	8.19	7.77	7.90	0.18	9.00
ZnSe	8.60	8.20	8.02	8.39	8.11	8.24	0.18	9.20
CdS	9.50	9.10	8.94	9.28	8.99	9.25	0.16	9.50
CdSe	9.70	9.20	9.05	9.42	9.20	9.41	0.15	10.04
GaN	17.00	16.60	15.81	16.53	16.00	16.53	0.79	17.00
GaP	18.30	17.80	16.77	17.21	17.00	17.40	1.03	18.55
GaAs	18.50	18.00	17.10	17.36	17.20	17.60	0.90	18.80
InP	16.90	16.30	16.64	16.97	16.72	16.99	−0.34	16.80

[1] P. E. Blöchl, Projector augmented-wave method, Physical Review B **50**, 17953 (1994).

[2] G. Kresse and J. Hafner, Ab initio molecular dynamics for liquid metals, Phys. Rev. B **47**, 558 (1993).

[3] G. Kresse and J. Furthmüller, Efficient iterative schemes for ab initio total-energy calculations using a plane-wave basis set, Physical Review B **54**, 11169 (1996).

[4] R. W. Nunes and X. Gonze, Berry-phase treatment of the homogeneous electric field perturbation in insulators, Physical Review B **63**, 155107 (2001).

[5] A. Grüneis, G. Kresse, Y. Hinuma, and F. Oba, Ionization potentials of solids: The importance of vertex corrections, Phys. Rev. Lett. **112**, 096401 (2014).

[6] J. Klimeš, M. Kaltak, and G. Kresse, Predictive *GW* calculations using plane waves and pseudopotentials, Phys. Rev. B **90**, 075125 (2014).

[7] W. Chen, G. Miceli, G. M. Rignanese, and A. Pasquarello, Nonempirical dielectric-dependent hybrid functional with range separation for semiconductors and insulators, Phys. Rev. Mater. **2**, 073803 (2018).

[8] W. Mönch, *Semiconductor Surfaces and Interfaces*, edited by G. Ertl, R. Gomer, H. Lüth, and D. L. Mills, Springer Series in Surface Sciences, Vol. 26 (Berlin, Heidelberg, 2001).

[9] T. Jaouen, G. Jézéquel, G. Delhaye, B. Lépine, P. Turban, and P. Schieffer, Work function shifts, Schottky barrier height, and ionization potential determination of thin MgO films on Ag(001), Applied Physics Letters **97**, 232104 (2010).

[10] A. Facchetti and T. J. Marks, eds., *Transparent Electronics: From Synthesis to Applications* (Chichester, UK, 2010).

[11] M.-S. Miao, S. Yarbro, P. T. Barton, and R. Seshadri, Electron affinities and ionization energies of Cu and Ag delafossite compounds: A hybrid functional study, Physical Review B **89**, 045306 (2014).